# Time Domain Simulation of Common Mode Ferrite Chokes at System Level

Alberto Gascón Bravo, Salvador G. Garcia, *Senior Member, IEEE*, Alejandro Muñoz Manterola, Manuel Añón-Cancela, Roberto Moreno, Kenan Tekbaş, and Luis D. Angulo

***Abstract*—This article introduces a comprehensive methodology for analyzing common-mode (CM) ferrite chokes in time-domain (TD) methods, employing lumped dispersive loads, and validates it through a typical test setup for cable crosstalk assessment. The analysis begins with the experimental characterization of CM choke material properties using a coaxial line fixture to obtain its constitutive parameters. Subsequently, a simplified lumped dispersive convolutional model is obtained, representing the impedance of the ferrite when placed on a location on the cable. The first approach adopts a multiconductor transmission line (MTL) model for the cables, solving them by a finite-difference (FDTD) space-time scheme. The second approach utilizes the classical full-wave Yee-FDTD method in conjunction with the thin-wire Holland model for cables. The accuracy of the proposed methods is evaluated by comparing simulations performed with MTL-FDTD and Holland-Yee FDTD, to experimental measurements, and results obtained with the the frequency-domain finite element method using a 3-D model of the ferrite with its constitutive parameters. Finally, the validity and performance of the methodologies are critically discussed.**

***Index Terms*—Common mode (CM) chokes, complex permeability, ferrite, finite differences time domain, finite element method (FEM), multitransmission lines, transmission lines.**

## I. Introduction

COMMON mode (CM) ferrite chokes are essential components used for electromagnetic compatibility (EMC) purposes of suppressing or mitigating conducted and radiated electromagnetic interference (EMI). In the design and development process of an electrical system incorporating the chokes, validated simulation tools are needed to predict their behavior, test different system scenarios, or make any corrections/redesign in the system. The system-level simulation of this electrically large-scale problem usually involves two steps: 1) to model the choke as a component; and 2) to implement the component model into the system design.

Several studies have addressed the CM ferrite models for the simulation at only a component level, with certain simplifications in their models, such as considering a small electrical size and including some complexities, such as taking into account self-parasitics between coil turns, the nonlinear and frequency-dependent behavior of the core material, or the possibility of deembedding impedance measurements from their fixture [1], [2], [3], [4], [5]. However, these models are inadequate to describe the electromagnetic properties of CM ferrite beads or chokes with a low number of turns. In addition, these components exhibit an impedance that deviates from the typical $+20\,\mathrm{dB/dec}$ trend of an ideal inductor at above a certain frequency, typically ranging from $100\,\mathrm{kHz}$ to $100\,\mathrm{MHz}$, decreases to a value between $+10\,\mathrm{dB/dec}$ to $-10\,\mathrm{dB/dec}$ [6]. This impedance behavior is quite different from classical models based on self-resonance [7] and can be attributed to a degradation in the magnetic permeability of the core material. For this reason, we use the permeability approximated by a frequency-dependent complex permeability having a constant real permeability up to a certain frequency, above which the real permeability decreases [8], [9], [10].

Once the CM ferrite chokes are modeled at a component level, the chokes can be incorporated into 3-D full-wave simulations of systems with large electric sizes, either in the frequency domain (FD) or in the time domain (TD). This task usually involves using some simplifying assumption on the component model, e.g., by extracting a frequency-dependent impedance that can be incorporated as a lumped element. From an EMC perspective, TD methods present some benefits over FD ones since they can usually be formulated in an explicit marching-on-in-time manner [11], [12], and they scale linearly with the electrical size. In contrast, frequency domain (FD) simulations require solving a global system of equations, typically scaling worse than linearly. Additionally, TD simulations can obtain broadband results with a single run allowing investigation of systems in which the problematic resonances are not known *a priori*. The problem

Manuscript received 15 May 2023; revised 13 July 2023; accepted 4 August 2023. Date of publication 11 September 2023; date of current version 13 December 2023. This work was supported in part by MCIN/AEI/10.13039/501100011033, in part by Spanish MICINN EU FEDER under Grant PID2019.106120RB.C33 and Grant PID2019.106120RB.C32, in part by EU Horizon2020 Research and Innovation Programme under Marie Sklodowska-Curie Action under Grant 101066571, and in part by Junta de Andalucia FEDER under Grant B-TIC-700-UGR20. Funding for open access charge: Universidad de Granada/CBUA. *(Corresponding author: Luis D. Angulo.)*

Alberto Gascón Bravo, Salvador G. Garcia, Alejandro Muñoz Manterola, and Luis D. Angulo are with the Department of Electromagnetism, University of Granada, 18071 Granada, Spain (e-mail: agascon@ugr.es; salva@ugr.es; almuma@ugr.es; lmdiazangulo@ugr.es).

Manuel Añón-Cancela is with the Electromagnetic Compatibility Area of the National Institute of Aerospace Technology, 28850 Madrid, Spain (e-mail: agnoncm@inta.es).

Roberto Moreno is with IKERLAN Technology Research Centre, Basque Research and Technology Alliance, 20500 Arrasate/Mondragón, Spain (e-mail: rmoreno@ikerlan.es).

Kenan Tekbaş is with the Department of Electromagnetism, University of Granada, 18071 Granada, Spain, and also with the Department of Electrical and Electronic Engineering, Amasya University, 05100 Amasya, Türkiye (e-mail: kenan.tekbas@ugr.es).

Color versions of one or more figures in this article are available at https://doi.org/10.1109/TEMC.2023.3309698.

Digital Object Identifier 10.1109/TEMC.2023.3309698

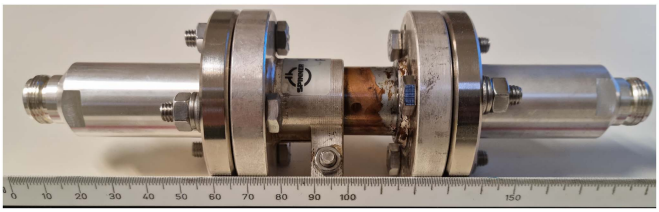

Fig. 1. Coaxial line experimental setup developed for the characterization of ferrite material.

of including TD models of CM chokes at system-level was addressed in [13]. In this reference the modeling of the choke is carried out by the inclusion of a volumic material with tailored dispersive properties. While this approach produces a reasonable accuracy it is problematic because the scales involved in the ferrite are much smaller than the system which forces to use a cell-size much smaller than the needed by the rest of the system. This limits severely the applicability of this technique, because it would force a global reduction of the time-step, with subsequent effects on the accuracy and computational performance. In contrast, the approach that we propose in this work does not force any change in the mesh and neither on the time-step, obtaining results which match experimental measurements and FD methods.

This work describes a roadmap for incorporating CM ferrite chokes into the system TD simulations using lumped components. We assume that we have no prior knowledge of the ferrite-specific properties; therefore, in Section II, we provide a method to extract a suitable model of its characteristics. In Section III, we describe how to incorporate the extracted model into simulations using different techniques both in TD and FD. In Section IV, we compare experimental results with the different simulation methods and discuss the results. Finally, Section V concludes the article.

## II. CM Choke Parameter Extraction

### A. Fixture Description

The coaxial line fixture of Fig. 1 was designed and built to characterize the ferrite. In contrast with the ones described in [14], [15], and [16], our approach has two ports, and it allows us to find the impedance from $S_{11}$ or $S_{21}$ measurements, presenting a higher sensitivity at low frequency ranges [17]. The fixture was made with a $50\,\Omega$ coaxial line made of copper, with an internal diameter $d_i = 8.7\,\mathrm{mm}$, external diameter of $d_o = 20\,\mathrm{mm}$ and length $h = 60\,\mathrm{mm}$. The line was terminated with two 7/8" flanges commercialized by Spinner [18]; one of the flanges was soldered to the line, while the other can be opened to introduce the device under test (DUT). The flanges are terminated in $50\,\Omega$ ports and connected to a Rohde & Schwarz ZNL6 vector network analyzer (VNA).

### B. Parameter Extraction

After loading a ferrite core into the fixture, the impedance $Z$ that it would present when used as a CM choke can be extracted

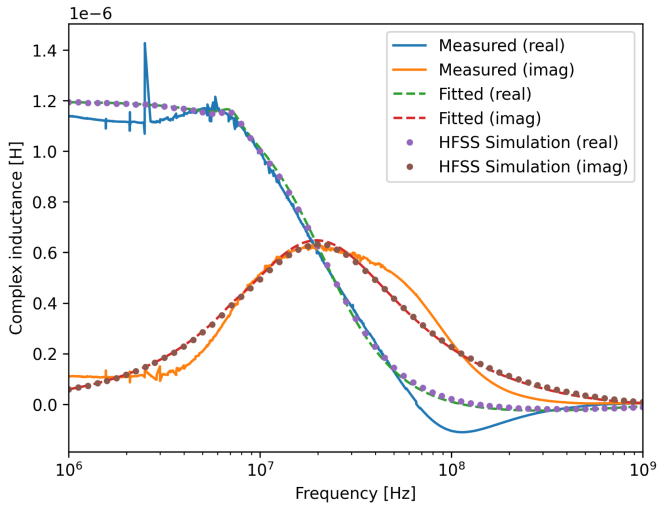


Fig. 2. Measured and fitted complex inductance for Würth 7427009 ferrite. A FEM simulation using Ansys HFSS was carried out to validate the assumptions made for the fitting.

from the measured scattering parameters by [17]

$$Z_{\text{meas.}} = Z_0 \frac{S_{21}}{2(1 - S_{21})} \tag{1}$$

with $Z_0 = 50\,\Omega$ being the impedance of the line. The *apparent* complex permeability of the ferrite core can be obtained from the impedance measurement using a procedure similar to the one described in [8].

To do this, we define a complex inductance $\boldsymbol{L}$, which can be derived from the measured impedance

$$\boldsymbol{L}_{\text{meas.}} = \frac{Z_{\text{meas.}}}{j\omega} \tag{2}$$

with $\omega$ being the angular frequency. The apparent complex magnetic permeability $\boldsymbol{\mu}$ is related to the complex inductance by

$$\boldsymbol{L}(\omega) = \boldsymbol{\mu}(\omega) \frac{\log(d_o/d_i)\, h}{2\pi}. \tag{3}$$

For certain ferrite materials, the electric conductivity and/or the imaginary part of the complex magnetic permeability can give rise to a skin effect that affects the impedance measurement [10]. This effect causes the apparent magnetic permeability derived in (3) to be different from the *intrinsic* permeability, which would be the one obtained discounting these dimensional effects. However, for the DUT studied in this work, the skin depth was much higher than the physical dimensions, allowing us to neglect these dimensional effects.

The data obtained from (1) cannot be used directly in a TD simulation as it is a discrete collection of data points that typically includes some experimental noise (e.g., Fig. 2). Additionally, TD simulations typically require transforming the FD data into functions that must be causal and passive. All these properties are ensured if we use a complex permeability

$$\boldsymbol{\mu}(\omega) = \mu' - j\mu'' \tag{4}$$

which is derived from physical assumptions and includes contributions from the natural spin resonance and domain-wall relaxation, with real and imaginary parts, respectively [9], [19].

$$\mu' = 1 + \frac{K_d\omega_d^2(\omega_d^2+\omega^2)}{(\omega_d^2-\omega^2)^2+\omega^2\beta^2} + \frac{K_s\omega_s^2\left[(\omega_s^2+\omega^2(1+\alpha^2))\right]}{\left[\omega_s^2-\omega^2(1+\alpha^2)\right]^2+4\omega^2\omega_s^2\alpha^2} \quad (5)$$

$$\mu'' = \frac{K_d\omega\beta\omega_d^2}{(\omega_d^2-\omega^2)^2+\omega^2\beta^2} + \frac{K_s\omega_s\omega\alpha\left[\omega_s^2+\omega^2(1+\alpha^2)\right]}{\left[\omega_s^2-\omega^2(1+\alpha^2)\right]^2+4\omega^2\omega_s^2\alpha^2} \quad (6)$$

$K_s$ is the static spin susceptibility, $K_d$ is the static susceptibility of the domain wall motion, $\omega_s$ is the spin resonance angular frequency, $\omega_d$ is the domain wall resonance angular frequency, with $\alpha$ and $\beta$ being damping factors. Therefore, the fitting problem reduces to finding the parameters $K_s$, $\omega_s$, $K_d$, $\omega_d$, and $\beta$ which minimize the following error metric:

$$\frac{1}{N}\sum_{n}^{N}\left|\boldsymbol{L}_{\text{meas.}}(\omega_n)-\boldsymbol{L}_{\text{fit}}(\omega_n)\right| \quad (7)$$

where $\boldsymbol{L}_{\text{meas.}}$ and $\boldsymbol{L}_{\text{fit}}$ are evaluated at each of the $N$ angular frequencies $w_n$ measured. $\boldsymbol{L}_{\text{fit}}$ is computed from (3) using the (4) for the permeability. In this work, the fitting procedure is carried out using a *basin-hopping* global optimization method [20] included in the Python scientific package *SciPy* [21].

### C. Validation and Results

The described procedure was applied to a commercially available NiZn ferrite (Würth 7427009 [6]) with physical dimensions compatible with the fixture. After performing a port-extension calibration on the VNA, the S-parameter measurements were converted to complex inductance using (1) and (2). Finally, the fitting procedure described in the previous section was carried out to minimize the error function (7). The results obtained after this process were: $K_d = 0.98$, $\omega_d = 44.7\,\text{Mrad/s}$, $\beta = 14.4\,\text{Mrad/s}$, $K_s = 338$, $\omega_s = 398\,\text{Mrad/s}$, and $\alpha = 3.19\,\text{rad/s}$. Fig. 2 shows the result of the measurements together with the fitting within its typical range of application (up to 1 GHz). The obtained permeability, deduced from (3), agrees with typical profiles reported in the literature [9], [16], [19].

The obtained permeability was used to perform a full-wave 3-D simulation of the fixture loaded with the ferrite, using the HFSS [22] FD finite element (FEM) solver. To do this, the inner part of the fixture was modeled as a PEC coaxial, with the $d_i$, $d_o$ and $h$ dimensions described before and terminated in two coaxial wave-ports. The choke itself was modeled as a volume and assigned a custom defined material with the fitted permeability. A very good fit compared to the model (3) is found; this corroborates that the magnetic skin effect is not playing a significant role in this case, further validating the assumptions made in the modeling.

## III. Simulation of CM Chokes At a System Level

### A. Multiconductor Transmission Line (MTL) Solver

The MTL method assumes a quasi-TEM propagation applicable in systems that can be decomposed on groups of conductors with constant cross-sections, i.e., translational symmetry. This assumption permits us to relate the voltages and currents on each conductor with per-unit-length parameters [23]. For a lossless line with $(N+1)$ conductors, these relationships can be expressed in the following form:

$$\begin{aligned}\partial_z\{\text{V}\} &= -[\text{R}]\{\text{I}\} - [\text{L}]\,\partial_t\{\text{I}\}\\ \partial_z\{\text{I}\} &= -[\text{G}]\{\text{V}\} - [\text{C}]\,\partial_t\{\text{V}\}\end{aligned} \quad (8)$$

with $\{\text{V}\}(z,t) = [V_1\, V_2\, \ldots\, V_N]^T$ being a vector of the voltages with respect to a conductor taken as ground and $\{\text{I}\}(z,t) = [I_1\, I_2\, \ldots\, I_N]^T$ is a vector of currents on each of these conductors. The matrices [L] and [C] represent the inductance and capacitance per unit length between all conductors. [R] and [G] represent the losses in the transmission line: resistance (along conductors) and conductance (between conductors) per unit length, respectively. Finally, (8) is discretized using the finite-difference time-domain technique (FDTD) described in [23], leading to the following voltage and current update equations:

$$\{\text{V}\}_k^{n+1} = \left(\frac{\Delta z}{\Delta t}[\text{C}] + \frac{\Delta z}{2}[\text{G}]\right)^{-1} \times \left[\left(\frac{\Delta z}{\Delta t}[\text{C}] - \frac{\Delta z}{2}[\text{G}]\right)\{\text{V}\}_k^n - \left(\{\text{I}\}_k^{n+1/2} - \{\text{I}\}_{k-1}^{n+1/2}\right)\right] \quad (9)$$

$$\{\text{I}\}_k^{n+3/2} = \left(\frac{\Delta z}{\Delta t}[\text{L}] + \frac{\Delta z}{2}[\text{R}]\right)^{-1} \times \left[\left(\frac{\Delta z}{\Delta t}[\text{L}] - \frac{\Delta z}{2}[\text{R}]\right)\{\text{I}\}_k^{n+1/2} - \left(\{\text{V}\}_{k+1}^{n+1} - \{\text{V}\}_k^{n+1}\right)\right] \quad (10)$$

where $\Delta t$ and $\Delta z$ are the time and space steps of the discretization, respectively, $k$ locates the voltage nodes and current segments along the discretized MTL, and $n$ locates the current time on the discretized solution time. The details of the implementation can be found in [24].

The quasi-TEM propagation assumption used by MTL allows to solve a wide variety of typical problems in EMC: crosstalk prediction, S-parameters extraction, susceptibility to radiated emissions, inclusion of nonlinear models, etc. Moreover, this allows a significant reduction in the complexity of the problem which directly translates into a significant computational efficiency. However, the quasi-TEM approach does not account electric fields aligned with the cables and therefore, cannot predict radiative effects, e.g., a radiating electric dipole.

The per-unit-length parameters in [R], [L], [G], and [C] depend on the frequency. However, for our purposes, we will assume that [L] and [C] are constant and that no losses between conductors exist, $[\text{G}] = 0$. The behavior of the choke will appear as an impedance $[\text{R}] = [\hat{Z}](z,\omega)$ dependent on the frequency and on the position. That is, $[\hat{Z}]$ is nonzero only at the position

where the lumped component is located. The introduction of the ferrite in the transmission line would make us treat the line as nonuniform and nonhomogeneous. However, the ferrite is considered to be a lumped element which does not modify the cross-section of the transmission-line, only its p.u.l impedance. According to [23], a nonuniform line in a homogeneous medium, whose cross-section does not change with distance, can be treated as a uniform line. With respect to the homogeneity of the line itself, we assume that the inhomogeneity introduced by the ferrite is small enough and can be neglected. The equation analogous to (8) in the frequency-domain is

$$\partial_z\{\hat{V}\} = -[\hat{Z}]\{\hat{I}\} - j\omega[\mathrm{L}]\{\hat{I}\}(z,\omega). \tag{11}$$

These frequency-domain relationships can be translated into the time domain convolutionally as

$$\begin{aligned}\partial_z\{\mathrm{V}\} &= -[\mathrm{Z}](z,t) * \{\mathrm{I}\}(z,t) - [\mathrm{L}]\,\partial_t\{\mathrm{I}\}\\ \partial_z\{\mathrm{V}\} &= -\int_0^t [\mathrm{Z}](z,\tau)\{\mathrm{I}\}(z,t-\tau) - [\mathrm{L}]\,\partial_t\{\mathrm{I}\}.\end{aligned} \tag{12}$$

To express (12) in a way that can be readily discretized and implemented into the FDTD scheme, we apply the piecewise linear recursive formulation proposed in [25]. In this formulation, a frequency-dependent magnitude is approximated by a rational representation (a sum of complex pole-residue pairs), obtained using the vector fitting technique [26], [27]. The inverse Fourier transform of this representation is a sum of exponentials whose convolution can be expressed recursively.

If the frequency-dependent impedance, whose value corresponds to the impedance extracted following the procedure described in Section II, is approximated by

$$\boldsymbol{Z}(s) = \boldsymbol{d} + s\boldsymbol{e} + \sum_i \frac{\boldsymbol{r}_i}{s-\boldsymbol{p}_i} + \sum_i \frac{\boldsymbol{r}_i^*}{s-\boldsymbol{p}_i^*} \tag{13}$$

where $s = j\omega$, and $\boldsymbol{r}_i$ and $\boldsymbol{p}_i$ are the $i$th residue and pole, respectively, and its time-domain equivalent can be written as follows:

$$\boldsymbol{Z}(t) = \boldsymbol{d}\delta(t) + \boldsymbol{e}\delta'(t) + \sum_i \boldsymbol{r}_i e^{\boldsymbol{p}_i\cdot t} \tag{14}$$

The convolutional term is then

$$\begin{aligned}\int_0^t [\mathrm{Z}](z,\tau)\{\mathrm{I}\}(z,t-\tau) &= \boldsymbol{d}\{\mathrm{I}\} + \boldsymbol{e}\partial_t\{\mathrm{I}\} +\\ &= \sum_i \boldsymbol{r}_i \int_0^t e^{\boldsymbol{p}_i\cdot t}\{\mathrm{I}\}(z,t-\tau).\end{aligned} \tag{15}$$

If (12) is discretized, the sum term in (15) takes the following form:

$$\sum_i \boldsymbol{r}_i \int_0^t e^{\boldsymbol{p}_i\cdot t}\{\mathrm{I}\}(z,t-\tau) = \sum_i \varphi_i^n \tag{16}$$

where

$$\begin{aligned}\varphi_i^n &= \{\mathrm{I}\}_k^{n+3/2} q_{1i} + \{\mathrm{I}\}_k^{n+1/2} q_{2i} + \varphi_i^n q_{3i}\\ q_{1i} &= \frac{\alpha_i}{\beta_i}\left(e^{\beta_i} - \beta_i - 1\right)\\ q_{2i} &= \frac{\alpha_i}{\beta_i}\left(1 + e^{\beta_i}(\beta_i - 1)\right)\\ q_{3i} &= e^{\beta_i},\quad \alpha_i = \frac{\boldsymbol{r}_i}{\boldsymbol{p}_i},\quad \beta_i = \boldsymbol{p}_i\,\delta t\end{aligned}$$

in which the convolution integral has been replaced by a recursive sum. Now, inserting (16) into (12) yields to the discretized update relation for $\{\mathrm{I}\}$, analogous to (10)

$$\begin{aligned}\{\mathrm{I}\}_k^{n+3/2} = F_1^{-1}\Big[F_2\{\mathrm{I}\}_k^{n+1/2} - (\{\mathrm{V}\}_{k+1}^{n+1} - \{\mathrm{V}\}_k^{n+1})\\ - \Delta z\sum_i q_{3i}\varphi_i^{n-1}\Big]\end{aligned} \tag{17}$$

where

$$F_1 = \left(\frac{\Delta z}{\Delta t}[\mathrm{L}] + \frac{\Delta z}{2}\boldsymbol{d} + \frac{\Delta z}{\Delta t}\boldsymbol{e} + \Delta z\sum_i q_{1i}\right) \tag{18}$$

$$F_2 = \left(\frac{\Delta z}{\Delta t}[\mathrm{L}] - \frac{\Delta z}{2}\boldsymbol{d} + \frac{\Delta z}{\Delta t}\boldsymbol{e} - \Delta z\sum_i q_{2i}\right). \tag{19}$$

### B. Full-Wave FDTD Solver

The full-wave FDTD method is widely used to analyze transient fields in 3-D. The standard version of this technique is based on tessellating the space with cubes known as Yee cells, locating the electric and magnetic fields in their edges and faces [28]. This staggered arrangement of the fields is evolved with a second-order leapfrog algorithm, which results in a scheme that has the following form (in free space, for simplicity):

$$\begin{aligned}\{E^{n+1}\} &= \{E^n\} + [A_H]\{H^{n+1/2}\} + \{S^{n+1/2}\}\\ \{H^{n+3/2}\} &= \{H^{n+1/2}\} + [A_E]\{E^n\}\end{aligned} \tag{20}$$

with $\{E\}$ and $\{H\}$ being the discretized fields in the Yee's cell and $\{S\}$ the discrete electric-source terms. $[A_H]$ and $[A_E]$ are sparse evolution matrices that take into account the finite-differences spatial semi-discretization and boundary conditions.

While this scheme is suitable for a wide range of applications, it has limitations when multiple geometrical scales are involved in a single problem. Therefore, to apply it to structures containing wires, the base algorithm can be modified with the well-known Holland method for thin wires [29], [30].

Holland's method employs for a thin wire the same equations (8) used in Section III, now for a single TL, by assuming, roughly speaking, that the surrounding space acts as a reference *current return* of the wire. The scalar inductance per unit length is $L = \langle\frac{\mu_0}{2\pi}\ln\rho\rangle$, related to the capacitance by $C = 1/(Lc^2)$, with $c$ the free-space light speed, and $\langle\cdot\rangle$ denoting some integral average around the thin wire (full details can be found in [29].)

The TL single-wire Holland's equations are discretized by an FDTD scheme. They are coupled with the Yee algorithm at the wire locations and at each time step in a two-way explicit manner: They use the FDTD E-fields as distributed voltage sources in Holland equations (independent terms added to (8), and return the currents as electric-source terms to the FDTD equations (20).

Incorporating the ferrite choke in the Holland model thin wire uses the same method described in Section III for the MTL case: A dispersive lumped impedance at the choke location. The only difference between the MTL and the full-wave Holland-FDTD method is how the wires communicate among themselves: By inductance and capacitance matrices or by Yee's algorithm explicitly propagating the electromagnetic fields by Maxwell equations.

However, in the solver we used for this article, we have implemented a slightly different algorithm based in [31] to simulate dispersive elements in terms of their admittance instead of their impedance. For this, a poles-residues fit to the element admittance is found equivalently to (13)

$$\boldsymbol{Y}(s) = \boldsymbol{d}' + s\boldsymbol{e}' + \sum_i \frac{\boldsymbol{r}'_i}{s - \boldsymbol{p}'_i} + \sum_i \frac{\boldsymbol{r}'^*_i}{s - \boldsymbol{p}'^*_i}. \tag{21}$$

As in (13), the admittance corresponds to the impedance extracted in Section II. The previous relationship allows us to interpret each term easily as follows: The constant and linear frequency terms are equivalent to a parallel RC circuit; each real-pole term is equivalent to a series RL circuit, and each pair of complex-conjugate poles is equivalent to a circuit composed by a series RL in series with a parallel RC.

## IV. Experimental and Simulation Results

### A. Experimental Setup

To test the validity of the models and procedures presented in Sections II and III, we have employed the cable panel fixture shown in Fig. 3(a). The panel is composed of two metallic brackets screwed to a metallic sheet. Three types of cable have been mounted between the brackets, from top to bottom: 1) A single wire with diameter $3\,\mathrm{mm}$; 2) a single wire with diameter $1\,\mathrm{mm}$; and 3) a twisted pair formed by two wires of $0.8\,\mathrm{mm}$. Eight N-type connectors (input or output ports) are placed, four on each side of the metallic holder. The opposite side ports are separated by $40\,\mathrm{cm}$, are elevated from the ground plate of $4\,\mathrm{cm}$, and the distance to neighboring ports is $5\,\mathrm{cm}$. The ferrite described in Section II is placed in the midpoint of the top wire. The S-parameters of the line were measured with the same VNA employed in Section II between $10\,\mathrm{MHz}$ to $1\,\mathrm{GHz}$.

### B. Simulations

This setup has been modeled and simulated using the MTL-FDTD method described in Section III-A, the full-wave FDTD method described in Section III-B, and the commercial full-wave frequency-domain Ansys HFSS 2019 solver [22]. Two sets of measurements and their corresponding simulations were made, one without choke and another using the ferrite one characterized in Section II.

The MTL-FDTD method employed in this work can be found in [24] as part of a larger open-source MTL network solver, which our team is currently developing. The wires were terminated in $50\,\Omega$ connectors mimicking the loads and port impedances of the experimental setup. The [L] and [C] matrices needed in (8) to model the MTL cross-section were obtained using the SACAMOS open-source software [32]. All conductors were considered perfect electric (PEC); therefore, per-unit-length loss terms were not included. The ferrite CM choke was modeled as a lumped impedance using (12) and fitting the dispersive permeability obtained in Section II.

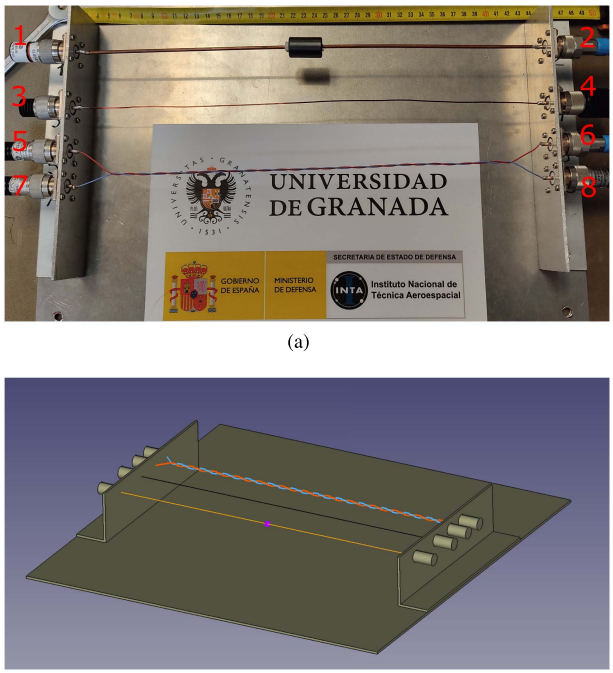


(a)



(b)

Fig. 3. Experimental setup measured (top) and CAD used for simulation (bottom) setups. (a) Cable panel with ferrite set in wire 1, including numbering of the ports. In this configuration, the VNA is connected to ports (2,6) while the rest of the ports are loaded with $50\,\Omega$ connectors. Similar configurations were made by connecting the VNA at ports (1,2) and (1,4), repeating the process after removing the ferrite from the wire. (b) CAD model of the experimental setup. The ferrite has been modeled as a dispersive connector in the midpoint between ports 1 and 2 (pink square in the figure).

The model was excited using a Gaussian voltage source and sampling the voltages and currents at the different ports. These voltages and currents were used to extract the S-parameters of the system.

For the full wave FDTD approach, we used the *SEMBA-FDTD* [33] software, which has been liberated recently as an open-source code and is available at [34]. *SEMBA-FDTD* is a state-of-the-art general-purpose time-domain simulator developed and validated by our team for various applications [35], [36]. The simulation setup is shown in Fig. 3(b). All elements in the panel except for the ferrite were modeled as PEC. The individual wires and the twisted pair have been modeled as a square double helix, using the thin wire approach described in Section III-B. The simulation grid to arrange Yee cells was selected so that the wires and the segments of the helices run along the grid lines. Two simulations have been performed, one without ferrite and one with ferrite. In the latter case, the ferrite was modeled as a dispersive lumped connector, with an impedance derived from (21). At each port, the current and voltage are sampled at regular time steps and used to derive the S-parameters that characterize the system.

TABLE I
CONSTANT TERM AND LIST OF POLES AND RESIDUES USED IN THE FIT OF THE FERRITE IMPEDANCE USING THE VECTOR FITTING TECHNIQUE

| Number | Pole | Residue |
|---|---|---|
| 1 | $-1.48535971 \cdot 10^{10}$ | $-9.32340577 \cdot 10^{11}$ |
| 2 | $-2.29904404 \cdot 10^{8}$ | $7.81078516 \cdot 10^{9}$ |
| 3 | $-6.73258119 \cdot 10^{7}$ | $9.49567177 \cdot 10^{8}$ |
| 4 | $-1.21476603 \cdot 10^{8}$ | $-2.28755419 \cdot 10^{10}$ |
| 5 | $-7.40969289 \cdot 10^{5} + 4.4929341 \cdot 10^{7} j$ | $1.49402382 \cdot 10^{6} + 6.74652 \cdot 10^{5} j$ |
| 6 | $-7.40969289 \cdot 10^{5} - 4.4929341 \cdot 10^{7} j$ | $1.49402382 \cdot 10^{6} - 6.74652 \cdot 10^{5} j$ |
| d | 203.087 | |

TABLE II
CONSTANT TERM AND LIST OF POLES AND RESIDUES USED IN THE FIT OF THE FERRITE ADMITTANCE USING THE VECTOR FITTING TECHNIQUE

| Number | Pole | Residue |
|---|---|---|
| 1 | $-7.9079328 \cdot 10^{9}$ | $8.6156480 \cdot 10^{6}$ |
| 2 | $-1.7434138 \cdot 10^{4}$ | $5.5376150 \cdot 10^{5}$ |
| 3 | $-1.4793911 \cdot 10^{8} + 1.1771422 \cdot 10^{8} j$ | $-2.65703626587 \cdot 10^{4} - 2.3006581 \cdot 10^{4} j$ |
| 4 | $-1.4793911 \cdot 10^{8} - 1.1771422 \cdot 10^{8} j$ | $-2.65703626587 \cdot 10^{4} + 2.3006581 \cdot 10^{4} j$ |
| d′ | 0.003625 | |

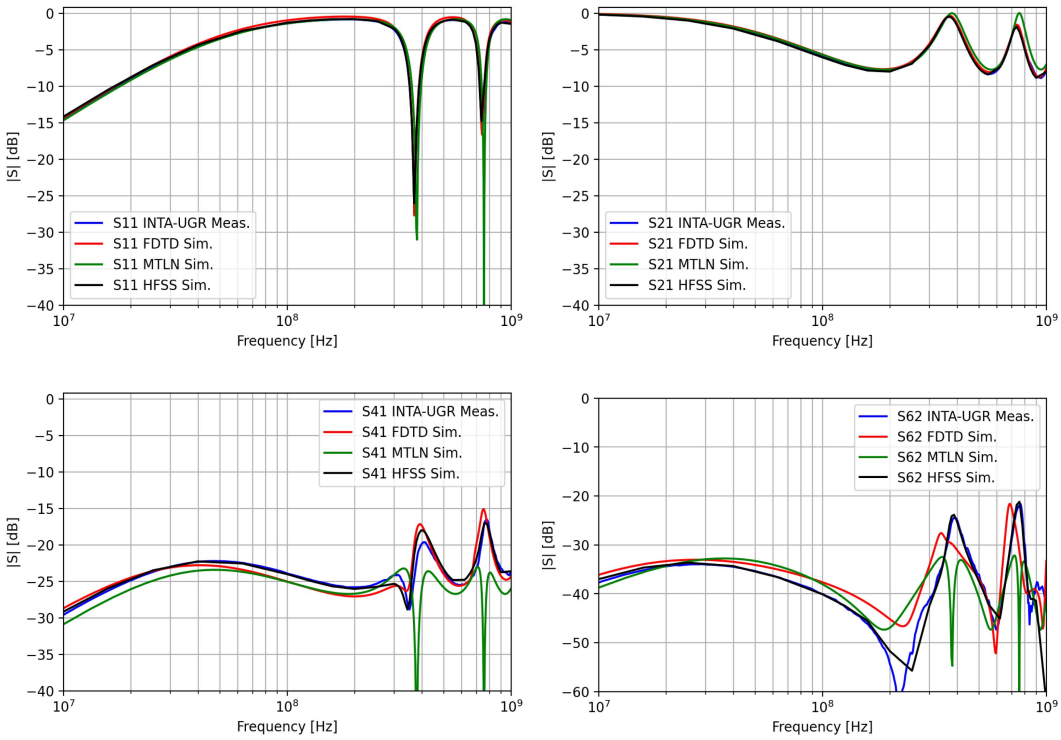


Fig. 4. Measurements and experimental results for the cable panel without ferrite.

The MTL-FDTD method (and the full-wave FDTD approach) require a rational approximation of the lumped element impedance (and admittance). The frequency-dependent impedance of the ferrite is computed from the permeability obtained from the parameter extraction procedure described in Section II as follows:

$$\boldsymbol{Z} = j\omega \boldsymbol{L}_{fit} \tag{22}$$

$$= j\omega \boldsymbol{\mu}_{fit} \ln\left(\frac{r_e}{r_i}\right) \frac{h}{2\pi} \tag{23}$$

$$= j\omega(\mu'_{fit} - j\mu''_{fit}) \ln\left(\frac{r_e}{r_i}\right) \frac{h}{2\pi} \tag{24}$$

where $r_e, r_i$, and $h$ are the outer radius, the inner radius, and the length of the ferrite, respectively, and $\mu'_f$ and $\mu''_f$ are the real and imaginary parts of the ferrite permeability. The rational approximations needed in (13) and (21) have been obtained using the vector fitting technique as implemented in [37] on this impedance, and the corresponding admittance $Y = Z^{-1}$. The poles and residues resulting from each fit are shown in Tables I and II.

All the materials present in the simulations were modeled as PEC, except the ferrite choke and the dielectric coating of the twisted wires. The choke was modeled as a volumic object and assigned with the fitted magnetic permeability obtained in Section II, whereas the coating was modeled as Teflon ($\varepsilon_r = 2.1$).

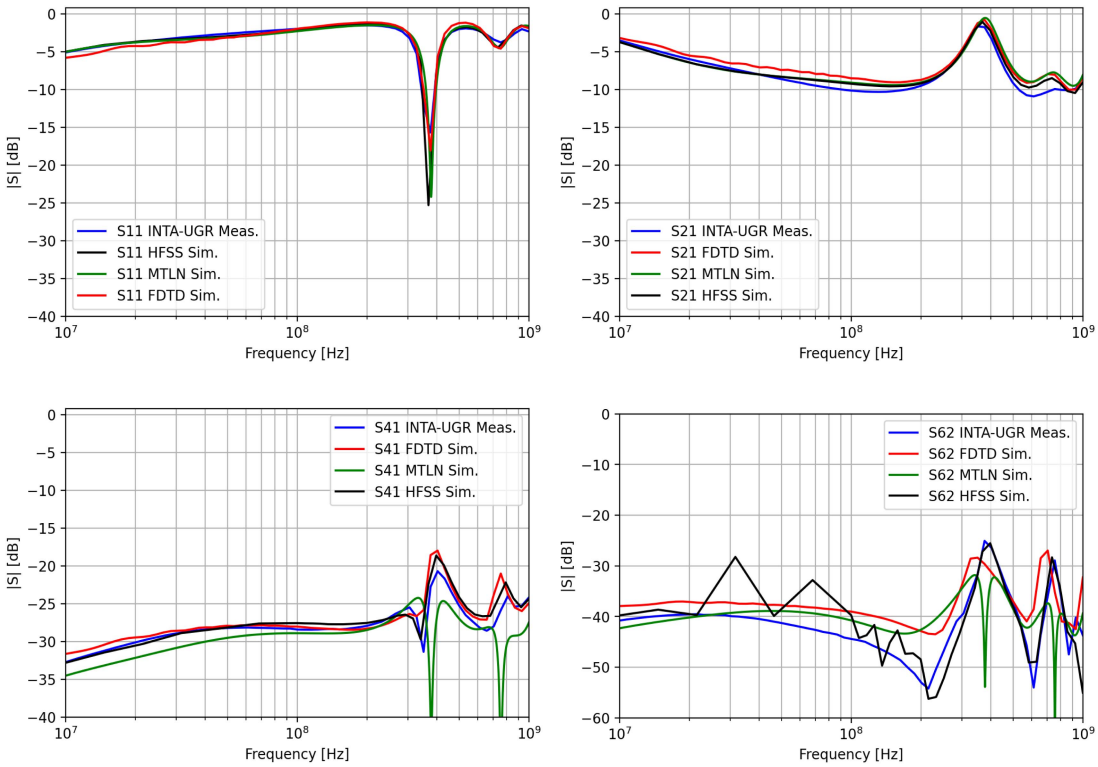


Fig. 5. Measurements and experimental results for the cable panel with the 7427009 ferrite located in the middle of the wire.

In the MTL-FDTD and full wave FDTD simulations, the ports were lumped, allowing us to extract S-parameters directly. In the HFSS simulation, eight wave ports were situated on the outer faces of each N-type connector, allowing a similar S-parameter extraction.

### C. Results Discussion

The magnitudes of the $S_{11}$, $S_{21}$, $S_{41}$, and $S_{62}$ parameters for the measurements and simulations carried out without and with ferrite are shown in Figs. 4 and 5, respectively. These ports were chosen as representative cases of reflection and transmission miss-match ($S_{11}$ and $S_{21}$) and crosstalk ($S_{41}$ and $S_{62}$).

For the case without ferrite, $S_{11}$ has an excellent agreement between the four methods. The $S_{21}$ result also shows a good agreement between the four methods, except in the region above $500\,\mathrm{MHz}$ for the MTL-FDTD method. This mismatch is probably caused by the fact that MTL does not consider radiative losses, which appear above the first resonance of the setup. FDTD and FEM are both full-wave and can adequately model that effect. The $S_{41}$ cases show a better agreement between measurements and full-wave simulations. MTL presents a slight offset at low frequencies caused by underestimating the mutual inductance between the loops formed by the first and second wires. The reasons for this offset might be the limitation of the validity of the translational symmetry assumed by the MTL approach or a lack of precision in extracting the per-unit-length inductance matrices. We do not find any reason for the peak inversion appearing in the two resonances of the MTL simulation. Finally, the $S_{62}$ parameters show a very good match with the FD FEM simulation. The FDTD methods agree with the results below $1\,\mathrm{MHz}$ but differ above that frequency. For the full wave FDTD method, this is very likely caused by the staircase modeling of the twisted pair.

For the case using ferrite, we obtain an excellent agreement for the $S_{11}$, $S_{21}$, and $S_{41}$ cases, highlighting the validity of the proposed approach. In the $S_{41}$, we observe a similar mismatch for the case without ferrite, possibly attributed to the same reasons. The $S_{62}$ does show an agreement as good as the previous ones. The problems that the FD FEM has are particularly noticeable by the noise appearing in the lower frequency band. We attribute this to a lack of convergence in that region caused by the intricate geometry of the twisted pair. The FDTD methods show a similar pattern as with the case with ferrite.

## V. Conclusion

In this work, we have provided a complete roadmap to simulate CM ferrite chokes. We describe a measurement fixture and a characterization method to obtain a complex inductance, from which we find a complex permeability using a fitting algorithm.

Once the ferrite is fully characterized, we have proposed two methods to incorporate it into a TD simulator as a lumped element with impedance/admittance expanded in a piecewise recursive convolutional algorithm. The first is an MTL-FDTD method, and the second is a full-wave FDTD algorithm. Both use a circuital lumped model, only differing in the wave propagator among the wires: either inductance and capacitance matrices or a full-wave solver. The lumped model results agree with experiments and full 3-D simulations of the ferrite geometry

performed with HFSS. As expected, above the first resonance, the full-wave solvers agree better with measurements than MTL, whereas for low-frequency, MTL provides enough accuracy.

Although a rigorous comparison of CPU times was not carried out in this work because different machines were used for the different simulations, MTL-FDTD runs are typically in the order of seconds, full wave FDTD in the order of minutes, and FD FEM is in the order of hours. This is indicative of the advantages that the proposed TD schemes can offer from an EMC design perspective.

## ACKNOWLEDGMENT

The authors would like to thank the National Institute of Aerospace Technology (INTA) for providing us with the experimental facilities to conduct the measurements used in this article. They also want to thank Würth Elektronik for providing the CM ferrite chokes and Rohde & Schwarz España, S.A. for the ZNL6 VNA used in the experimental measurements.

## REFERENCES

[1] C. R. Paul, *Introduction to Electromagnetic Compatibility*. New York, NY, USA: Wiley, 2006.
[2] C. Domínguez-Palacios, J. Bernal, and M. M. Prats, "Characterization of common mode chokes at high frequencies with simple measurements," *IEEE Trans. Power Electron.*, vol. 33, no. 5, pp. 3975–3987, May 2018.
[3] C. R. Sullivan and A. Muetze, "Simulation model of common-mode chokes for high-power applications," *IEEE Trans. Ind. Appl.*, vol. 46, no. 2, pp. 884–891, Mar./Apr. 2010.
[4] N. Moonen, R. Vogt-Ardatjew, A. Roc'h, and F. Leferink, "3-D full-wave high frequency common mode choke modeling," *IEEE Trans. Electromagn. Compat.*, vol. 62, no. 3, pp. 707–714, Jun. 2020.
[5] X. Liu et al., "Behavioral modeling of complex magnetic permeability with high-order Debye model and equivalent circuits," *IEEE Trans. Electromagn. Compat.*, vol. 63, no. 3, pp. 730–738, Jun. 2021.
[6] W. E. eiSos GmbH, "Datasheet we-fi leaded toroidal line choke," Tech. Rep., 2020. [Online]. Available: https://www.we-online.com/components/products/datasheet/7427009.pdf
[7] J. Eco and A. Limjoco, "Ferrite bead demystified," Application Note AN-1368, 2016. Accessed: Mar. 17, 2017, Available online: https://www.analog.com/media/en/technical-documentation/application-notes/AN-1368.pdf
[8] E. S. Lee and B. G. Choi, "Calculation methodologies of complex permeability for various magnetic materials," *Electronics*, vol. 10, no. 17, 2021, Art. no. 2167.
[9] A. Barba, C. Clausell, J. Jarque, and L. Nuño, "Magnetic complex permeability (imaginary part) dependence on the microstructure of a Cu-doped Ni–Zn-Polycrystalline sintered ferrite," *Ceramics Int.*, vol. 46, no. 10, pp. 14558–14566, 2020. [Online]. Available: https://www.sciencedirect.com/science/article/pii/S0272884220305812
[10] M. Kacki, M. S. Rylko, J. G. Hayes, and C. R. Sullivan, "Analysis and experimental investigation of high-frequency magnetic flux distribution in Mn-Zn ferrite cores," *IEEE Trans. Power Electron.*, vol. 38, no. 1, pp. 703–716, Jan. 2023.
[11] A. Taflove, A. Oskooi, and S. G. Johnson, *Advances in FDTD Computational Electrodynamics: Photonics and Nanotechnology*. Norwood, MA, USA: Artech House, 2013.
[12] L. D. Angulo, J. Alvarez, M. F. Pantoja, S. G. Garcia, and A. R. Bretones, "Discontinuous Galerkin time domain methods in computational electrodynamics: State of the art," *Forum Electromagn. Res. Methods Appl. Technol.*, vol. 10, no. 4, pp. 1–24, 2015. [Online]. Available: http://www.e-fermat.org/files/articles/Angulo-ART-2015-Vol10-Jul_Aug-004%20Discontinuous%20Galerkin%20Time%20%20....pdf
[13] J. Xu et al., "Complex permittivity and permeability measurements and finite-difference time-domain simulation of ferrite materials," *IEEE Trans. Electromagn. Compat.*, vol. 52, no. 4, pp. 878–887, Nov. 2010.
[14] A. Stadler, M. Albach, and A. Lindner, "A practical method to measure electrical ac conductivity of mnzn ferrites using conventional toroids," *IEEE Trans. Magn.*, vol. 46, no. 2, pp. 678–681, Feb. 2010.
[15] Agilent, "Application note 1369-1 solutions for measuring permittivity and permeability with LCR meters and impedance analyzers," Tech. Rep., 2003. [Online]. Available: https://www.keysight.com/us/en/assets/7018-06683/application-notes/5980-2862.pdf
[16] J. Xu et al., "Measurement of electromagnetic parameters and fdtd modeling of ferrite cores," in *Proc. IEEE Int. Symp. Electromagn. Compat.*, 2009, pp. 83–88.
[17] R. Dosoudil, "Determination of permeability from impedance measurement using vector network analyzer," *J. Elect. Eng.*, vol. 63, no. 7, pp. 97–101, 2012.
[18] Spinner, "Rigid line components 7/8 in SMS," Tech. Rep. [Online]. Available: https://products.spinner-group.com/Downloads/Spinner/CB-L-176-177-DS.pdf
[19] T. Tsutaoka, "Frequency dispersion of complex permeability in Mn–Zn and Ni–Zn spinel ferrites and their composite materials," *J. Appl. Phys.*, vol. 93, no. 5, pp. 2789–2796, 2003.
[20] D. J. Wales and J. P. Doye, "Global optimization by basin-hopping and the lowest energy structures of lennard-jones clusters containing up to 110 atoms," *J. Phys. Chem. A*, vol. 101, no. 28, pp. 5111–5116, 1997.
[21] P. Virtanen et al., "SciPy 1.0: Fundamental algorithms for scientific computing in python," *Nature Methods*, vol. 17, pp. 261–272, 2020.
[22] Ansys, "HFSS," [Online]. Available: https://www.ansys.com/products/electronics/ansys-hfss
[23] C. R. Paul, *Analysis of Multiconductor Transmission Lines*. New York, NY, USA: Wiley, 2007.
[24] OpenSEMBA, "MTLN." [Online]. Available: https://github.com/OpenSEMBA/mtln
[25] K. S. Oh and J. Schutt-Aine, "An efficient implementation of surface impedance boundary conditions for the finite-difference time-domain method," *IEEE Trans. Antennas Propag.*, vol. 43, no. 7, pp. 660–666, Jul. 1995.
[26] B. Gustavsen and A. Semlyen, "Rational approximation of frequency domain responses by vector fitting," *IEEE Trans. Power Del.*, vol. 14, no. 3, pp. 1052–1061, Jul. 1999.
[27] B. Gustavsen, "Improving the pole relocating properties of vector fitting," in *Proc. IEEE Power Eng. Soc. Gen. Meeting*, 2006, pp. 1–pp.
[28] K. Yee, "Numerical solution of initial boundary value problems involving Maxwell's equations in isotropic media," *IEEE Trans. Antennas Propag.*, vol. 14, no. 3, pp. 302–307, May 1966.
[29] R. Holland and L. Simpson, "Finite-difference analysis of EMP coupling to thin struts and wires," *Electromagn. Compat., IEEE Trans.*, vol. EMC-23, no. 2, pp. 88–97, May 1981.
[30] S. Schmidt and G. Lazzi, "Use of the FDTD thin-strut formalism for biomedical telemetry coil designs," *IEEE Trans. Microw. Theory Techn.*, vol. 52, no. 8, pp. 1952–1956, Aug. 2004.
[31] G. Antonini, "SPICE equivalent circuits of frequency-domain responses," *IEEE Trans. Electromagn. Compat.*, vol. 45, no. 3, pp. 502–512, Aug. 2003.
[32] ESA, George Green Institute, University of Nottingham, NLR, "SACAMOS, state-of-the-art CAble MOdels for spice," [Online]. Available: https://http://www.sacamos.org/
[33] S. G. Garcia et al., "SEMBA–EMC Broadband Simulator," Tech. Rep., 2015. [Online]. Available: https://www.sembahome.org/
[34] OpenSEMBA, "FDTD," [Online]. Available: https://github.com/OpenSEMBA/fdtd
[35] M. R. Cabello et al., "SIVA UAV: A case study for the EMC analysis of composite air vehicles," *IEEE Trans. Electromagn. Compat.*, vol. 59, no. 4, pp. 1103–1113, Aug. 2017.
[36] L. D. Angulo, M. R. Cabello, J. Alvarez, A. R. Bretones, and S. G. Garcia, "From microscopic to macroscopic description of composite thin panels: A roadmap for their simulation in time domain," *IEEE Trans. Microw. Theory Techn.*, vol. 66, no. 2, pp. 660–668, Feb. 2018.
[37] A. Arsenovic et al., "SCIKIT-RF: An open source python package for microwave network creation, analysis, and calibration [speaker's corner]," *IEEE Microw. Mag.*, vol. 23, no. 1, pp. 98–105, Jan. 2022.

**Alberto Gascón Bravo** received the M.Sc. and Ph.D. degrees in physics from the University of Granada, Granada, Spain, in 2009 and 2014, respectively.

He is currently a Postdoctoral Researcher with the Department of Electromagnetism and Matter Physics, the University of Granada. He has worked in the fields of astroparticle physics and accelerator physics. His current research interests include electromagnetic compatibility, computational electromagnetism, and material analysis.

**Salvador G. Garcia** (Senior Member, IEEE) received the M.Sc. and Ph.D. degrees (with extraordinary award) in physics from the University of Granada, Granada, Spain, in 1989 and 1994, respectively.

He cofounded the startup Elemwave devoted to numerical solver development and EM consultancy in 2010. He is a Full Professor with the Department of Electromagnetism and Matter Physics, University of Granada. He has authored or coauthored more than 90 refereed journal articles and book chapters and led several national and international projects. His current research interests include computational electromagnetics, electromagnetic compatibility, RCS, antenna design, and material analysis.

**Alejandro Muñoz Manterola** received the M.Sc. degree in material science from the University of Oviedo, Oviedo, Spain, in 2019. He is currently working toward the Ph.D. degree in computational electromagnetism with the University of Granada, Granada, Spain. He has been granted a FPI scholarship.

He is an Assistant Professor with the Department of Electromagnetism and Matter Physics, University of Granada. His current research includes computational electromagnetics, electromagnetic compatibility, and material analysis.

**Manuel Añón-Cancela** received the M.Sc degree in physics from the University of Santiago de Compostela, Santiago, Spain, in 1989.

He joined as E3 Test Engineer and is currently the Head of the Electromagnetic Compatibility Area of the National Institute of Aerospace Technology (INTA), Madrid, Spain, being involved in several national and international projects for the aerospace and defence sectors in 1991.

Mr. Añón-Cancela is a member of national and international standardization groups for military and civilian E3 specs.

**Roberto Moreno** was born in Eibar, Spain, in May 1974. He received the B.S. degree in electronic engineering from Mondragon Unibertsitatea, Mondragón, Spain, in 1998.

Since 1998, he has been with the Department of Electronics (now Hardware Systems and Communications Area), Ikerlan Research Center, Arrasate/Mondragón, Spain. Since 2008, he is the Head of EMC and nonfunctional requirements laboratory and Researcher. His current research interests include electrical and electronic behavior analysis and simulation of power and control electronics in the EMC area.

**Kenan Tekbaş** received the M.Sc. degree in communication engineering and the Ph.D. degree in electrical and electronic engineering from The University of Manchester, Manchester, U.K., in 2012 and 2017, respectively.

He is currently a Researcher with the Department of Electromagnetism, University of Granada, Granada, Spain, holding the position of Marie Skłodowska-Curie Fellow. His research interests include the finite-difference time-domain method, magnetic materials, subcell modeling techniques, computational electromagnetics, bioelectromagnetism, and high-performance computing.

**Luis Diaz Angulo** received the M.Sc. and Ph.D. degrees in physics from the University of Granada (UGR), in 2008, and 2014, respectively, and the M.Sc. degree in electronics engineering from the University of Granada, in 2015.

He is currently Associate Professor with the Department of Electromagnetism and State Matter, University of Granada (UGR), Granada, Spain. He has worked in time domain computational electromagnetics, especially discontinuous Galerkin and finite-differences. His research interests include electromagnetic compatibility and material characterization.